RAA 2020 Vol. **20** No. **11**, 169(13pp) doi: 10.1088/1674-4527/20/11/169

http://www.raa-journal.org *http://iopscience.iop.org/raa*

***R**esearch in*
***A**stronomy and*
***A**strophysics*

The local and global properties of different types of supernova host galaxies

Li Zhou[1,2], Yan-Chun Liang[2], Jun-Qiang Ge[2], Yi-Nan Zhu[1], Xu Shao[2], Hong Wu[2], Wei-Bin Shi[3] and Li-Cai Deng[2]

[1] Department of Astronomy, School of Physics and Astronomy, Sun Yat-sen University, Zhuhai 519082, China; *zhouli59@mail.sysu.edu.cn*
[2] National Astronomical Observatories, Chinese Academy of Sciences, Beijing 100101, China; *ycliang@nao.cas.cn*
[3] Shandong Provincial Key Laboratory of Optical Astronomy and Solar-Terrestrial Environment, School of Space Science and Physics, Shandong University at Weihai, Weihai 264209, China

Received 2020 January 20; accepted 2020 April 22

Abstract By using Data Analysis Pipeline (DAP) products of Mapping Nearby Galaxies at Apache Point Observatory (MaNGA), which are publicly available from the SDSS Data Release 15, we analyze the local properties at the SN explosion sites and global properties of different types of SN host galaxies to explore the explosion environments of different types of SNe. In our sample, there are 67 SN host galaxies in the field of view of MaNGA, including 32 Type Ia, 29 core collapse SNe (CCSNe), 1 superluminous SN (SLSN), 1 Type I and 4 unclassified type of SNe, with which we can apply the K-S test for analysis and derive statistically robust results. Due to the limited sample size, we could not remove the mass dependence in this work, which is likely the true driver of the trends for the properties presented in this work. The global star formation rate (SFR) and EW(Hα) for SN Ia hosts are slightly lower than those for CCSN hosts on average. SN Ia host galaxies are $\sim$0.3 dex more massive than CCSN hosts, which implies that the number ratio of CCSNe to Type Ia SNe will decrease with increasing stellar mass of host galaxies. The stellar population age of SN Ia host galaxies is older than that of CCSN hosts on average. There is no significant difference between different types of SN hosts for some properties, including local SFR density (ΣSFR), and local and global gas-phase oxygen abundance. For most galaxies in our sample, the global gas-phase oxygen abundance estimated from the integrated spectra of SN hosts can represent the local gas-phase oxygen abundance at the SN explosion sites with small bias.

Key words: galaxies: abundances — galaxies: general — galaxies: stellar content — supernovae: general — techniques: spectroscopic

1 INTRODUCTION

As one of the most violent and important processes, supernova (SN) explosions mark the death of a star's life. Supernovae (SNe) can be classified into several types according to their different spectral features (Filippenko et al. 1997; Hamuy et al. 2002; Turatto et al. 2003; Barbon et al. 1979; Rubin et al. 2016; Schlegel 1990).

A star with an initial stellar mass less than $8\ M_{\odot}$ will produce a degenerate carbon-oxygen (CO) white dwarf, which can grow by accreting materials from its non-degenerate companion star. When its mass increases to $1.4\ M_{\odot}$, a Type Ia SN (SN Ia) is produced after a bright thermonuclear explosion (Becker & Iben 1980; Hoyle & Fowler 1960). SNe Ia are considered as standard candles and are employed for calculating cosmological distances. They have been utilized to make great contributions in the discovery of dark matter and the accelerating expansion of the Universe (Riess et al. 1998; Perlmutter et al. 1999). Once a star has its initial mass larger than $8\ M_{\odot}$, an explosion caused by the gravitational collapse will happen and leave a neutron star or black hole as the remnant (Bethe et al. 1979; Arnett et al. 1989). This Core-Collapse supernova (CCSN) includes Type Ib, Ic and II SNe.

Many efforts have been devoted to study the correlations between different types of SNe and their host galaxies by applying single fiber spectra (Han et al. 2010; Kelly et al. 2012; Prieto et al. 2008; Shao et al. 2014). With the development of integral field spectroscopy (IFS) on modern telescopes, the local environment of SNe

and their host galaxies can be investigated with IFS observations of SN host galaxies (Stanishev et al. 2012; Kuncarayakti et al. 2013a,b; Galbany et al. 2016a).

Many works focusing on the SN host galaxies have performed statistical analysis on the local and global properties of different types of SN host galaxies. Galbany et al. (2014) studied 95 different types of SNe hosted in 81 galaxies using IFS of the Calar Alto Legacy Integral Field Area (CALIFA), the PPAK IFS Nearby Galaxies Survey (PINGS) and some other observations. Galbany et al. (2016b) obtained a larger number of SN host galaxies (115) and analyzed their metallicity with IFS data. With both IFS and long-slit data, Lyman et al. (2018) studied the environment of 37 SNe Iax (SN Iax is a peculiar class of SN that differs from normal SNe Ia) explosion sites and their host galaxies. Kuncarayakti et al. (2018) also considered IFS data to analyze the properties of 83 nearby CCSN explosion sites. Based on the IFS observations from PMAS/PPak Integral-field Supernova hosts COmpilation (PISCO), Galbany et al. (2018) investigated the local and global properties of 232 SN host galaxies, which hosted 272 SNe.

There are several works that examined the environment of SN explosion sites for a small sample using the Mapping Nearby Galaxies at Apache Point Observatory (MaNGA, Bundy et al. 2015). With MaNGA IFU data, Chen et al. (2017) and Izzo et al. (2018) analyzed the local environment of SLSN 2017egm in detail, which is one of the most nearby superluminous supernovae (SLSNe). Zhou et al. (2019) selected 11 SNe host galaxies from MaNGA Data Release (DR)13 and provided detailed information on the local and global properties of SN explosion sites and their host galaxies one by one.

In this paper, we will enlarge the sample size and analyze the differences of the local and global properties for different types of SN host galaxies (32 Type Ia, 29 CCSNe, 1 SLSN, 1 Type I and 4 unclassified types) by utilizing their MaNGA IFS observations to derive a more statistically robust conclusion. Also, we will compare the gas-phase oxygen abundance in the region of SNe explosion sites with those of the global regions of the host galaxies. Most of our sample galaxies have redshifts around 0.03 following the sample selection of MaNGA, which are systematically higher than other samples established in previous works.

The paper is organized as follows: in Section 2, we introduce the sample selection method applied to select our SN host galaxies. We arrange the comparisons of the local and global properties of environment for different types of SN host galaxies in Section 3. Finally, we will discuss our results in Section 4 and conclude in Section 5. Throughout this paper, we adopt a cosmological model with $H_0 = 70\ \mathrm{km\,s^{-1}\,Mpc^{-1}}$, $\Omega_M = 0.3$ and $\Omega_\Lambda = 0.7$.

2 SAMPLE SELECTION AND DATA REDUCTION

We cross-correlate ∼4600 galaxies in the Sloan Digital Sky Survey (SDSS) DR15 (Aguado et al. 2019; Westfall et al. 2019) with Asiago Supernova Catalogue (ASC), Sternberg Astronomical Institute (SAI) supernova catalogue and supernovae in Transient Name Server (TNS) website. The detailed sample selection procedures are described as follows.

2.1 Supernova Catalogs

With its development, ASC has presented the information on more and more SNe and host galaxies through several years (Barbon et al. 1984, 1989, 1999). Although the last input of ASC was 2017jmj, which was discovered on 2017 December 31, ASC will check and update information on the listed SNe and their host galaxies. Detailed information on ASC is presented in *http://graspa.oapd.inaf.it/*.

The last modified version of SAI was on 2014 October 17 and there were 6545 SNe in this catalog. See detailed information on the SAI supernova catalogue in *http://www.sai.msu.su/sn/sncat/*.

TNS is an official mechanism of IAU and it reports new astronomical transient events. Once a transient event is spectroscopically confirmed, this new SN discovery will be officially named in the form of the naming rules established by IAU. Before being spectroscopically classified, the transient event has a prefix of 'AT'. If it is classified into any type of SN, the prefix will be changed into 'SN'. There have been 3967 classified SNe released by TNS to the public from 2016 January 1 to 2019 August 31. See detailed information on TNS in *https://wis-tns.weizmann.ac.il/*.

2.2 MaNGA DAP Data Products

MaNGA is one of three core programs of SDSS-IV and is designed to observe 10 000 galaxies with IFS. The survey covers galaxies with redshift ranging from 0 to 0.15, and stellar mass from $10^9\ M_\odot$ to $10^{11}\ M_\odot$, which can help clarify the galaxy evolution processes from birth, growth and finally death (Weijmans & MaNGA Team 2016; Bundy et al. 2015; Law et al. 2015; Drory et al. 2015; Blanton et al. 2017). MaNGA galaxies are divided into two kinds of samples based on their spatial coverage, i.e., the Primary sample for 2/3 and the Secondary sample for 1/3 of galaxies, which can cover galaxies out to $1.5\ R_e$ and $2.5\ R_e$, with median redshifts of 0.03 and 0.045, respectively (more details are in Bundy et al. 2015; Law et al. 2015; Wake et al. 2017; Yan et al. 2016).

The MaNGA Data Analysis Pipeline (DAP) was initially developed in 2014 with an original IDL version

and applied as a survey-level pipeline to provide data products to the SDSS collaboration. It has been evolved through several years to a Python implementation and is now flexible for prospective users (Aguado et al. 2019; Westfall et al. 2019). The MaNGA DAP products provide galaxy parameters extracted from both emission and absorption lines (Westfall et al. 2019), including spectral indexes, emission-line properties, gas and stellar kinematics, etc.

2.3 Cross-correlations of Catalogs and Final Sample

To obtain SN host galaxies in the field of view (FoV) of MaNGA, we match the R.A. and Dec. of SNe in ASC, SAI supernova catalogue and TNS with the R.A and Dec. of more than 4600 galaxies in SDSS DR15. The cross-match radius is set to 15″ to match the largest FoV of MaNGA. Then we draw the 2D maps and exclude galaxies in which the SNe are located out of the FoV of MaNGA. Finally, we select 67 SN host galaxies in this matching radius that have been observed. Table 1 presents detailed information. The '+' or '-' symbols in the table signify that there are active galactic nuclei (AGNs) or there are no AGNs in the galaxy centers respectively according to the Baldwin, Phillips and Terlevich (BPT) diagram, and more details will be described in Section 3.1. Through this table, we can see that there are 32 Type Ia SNe, 29 CCSNe, 1 SLSN (2017egm), 1 Type I SN and 4 unclassified SNe.

Figure 1 shows the range of redshift (z) and absolute magnitude in the r band (M_r, which is taken from MaNGA DRP) for our 67 sample galaxies marked by crosses and DR15 MaNGA galaxies marked by grey dots. The gap in this figure results from the sample selection of MaNGA, which includes Primary and Secondary Samples (Wake 2015; Belfiore et al. 2016). From this figure, we can see that the majority of SN host galaxies come from the Primary Sample, and very few come from the Secondary Sample. There are two possible reasons that may cause this effect. The first possible reason is the number ratio of the Primary and Secondary Samples of MaNGA. The Primary Sample is for 2/3 and the Secondary sample for 1/3 of MaNGA galaxies. The second possible reason is the range of the redshift of SN host galaxies. The median redshift for observed SNe is about 0.03, while the median redshifts of the Primary Sample and Secondary Sample are 0.03 and 0.045, respectively. Therefore, we may obtain more galaxies from the Primary Sample after cross-correlating with the SN catalogs. According to this figure, the redshifts in our sample galaxies range from 0.01 to 0.12 with a median value of about 0.03, and the M_r of all the 67 sample galaxies range from –23 to –18 mag. From the histogram in Figure 2, we can see that the redshifts of most

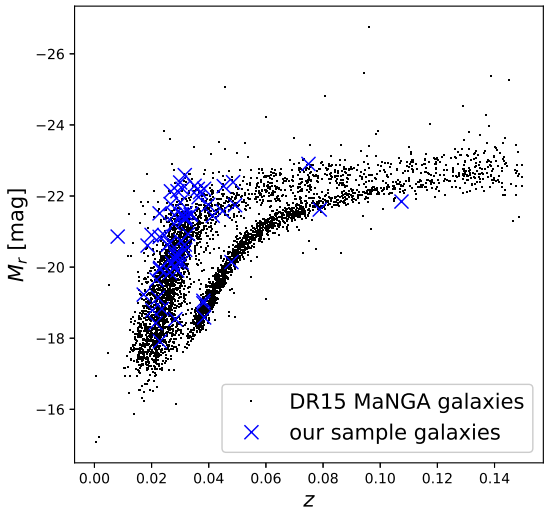

Fig. 1 The redshift and absolute magnitude in r band distributions for all the 67 sample galaxies compared with the DR15 MaNGA sample galaxies.

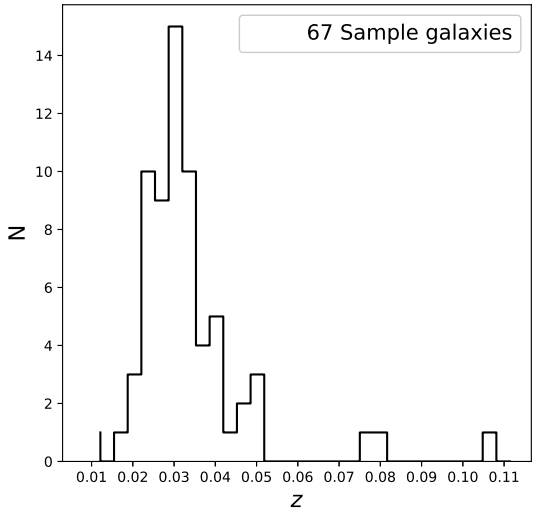

Fig. 2 The redshift distributions for all the 67 sample galaxies.

sample galaxies are located around 0.03. Table 1 presents the details of the redshift for each sample galaxy.

2.4 Parameter Estimations

In our work, we examine the emission line fluxes from MaNGA DAP to obtain the properties of dust extinction, star formation rate (SFR) and gas-phase oxygen abundance. The methods for calculating dust extinction, SFR and gas-phase oxygen abundance in this work are the

Table 1 Basic information from MaNGA and ASC on our 67 sample galaxies. The '+' symbols mean that there is an AGN in the galactic nucleus and '-' symbols signify that there is no AGN in the galactic nucleus.

Plateifu	SN Name	SN type	SN ra [deg]	SN dec [deg]	Host Name	Redshift	$E(B-V)$ [mag]	NSA$_{b/a}$	NSA$_{PA}$	AGN
8084–12702	2019abu	II	50.536613	–0.84006111		0.0364594	0.0656572	0.860265	47.9614	+
9871–12702	2018lev	II	228.28404	41.2637		0.0290635	0.0214573	0.545892	160.221	+
8080–12703	2018jfp	II	49.484488	–0.16970556		0.0227967	0.0727471	0.704163	61.6702	+
8257–12701	2018hfc	IIP	165.49408	45.227539		0.0199963	0.00869303	0.580468	72.7335	-
9872–9102	2018fbh	Ia	234.13327	41.799897		0.0413954	0.0331264	0.808343	120.581	+
8262–6104	2018ddh	Ia	184.68351	44.781975		0.0383413	0.0124629	0.620135	121.685	+
8602–12701	2018ccl	Ia	247.04635	39.820131		0.0267882	0.00939909	0.649031	2.06161	+
8945-9102	2018btb	Ia	173.61624	46.362531		0.0338424	0.0182859	0.839694	115.388	-
8611–6101	2018bbz	Ia	261.96804	60.096056	PGC 60339	0.0278347	0.0259684	0.840635	59.5055	+
8448–6102	2018aex	II	165.18908	22.2875		0.0229026	0.0173848	0.223525	117.637	-
8315–12704	2018aej	Ia	236.09589	39.558094		0.0479339	0.0165416	0.255403	175.803	-
8083–12704	2017jcu	II	50.695417	0.14808333	UGC 02705	0.0228308	0.124875	0.894133	154.66	+
8147–12701	2017ixz	IIb	116.76261	26.773825		0.0235924	0.0377963	0.649183	112.922	-
9029-6102	2017frc	II	246.39147	41.682189		0.0279312	0.00923756	0.968164	68.0598	-
8616–12702	2017fel	Ia	322.30573	–0.29470278		0.0305366	0.0524228	0.775617	76.7474	+
9095-6102	2017ets	Ia	243.44229	22.916428		0.0319161	0.0903559	0.684788	161.49	-
8454–12703	2017egm	SLSN-I	154.77342	46.453911		0.0307213	0.0113688	0.796432	5.52863	-
9872–12703	2017dit	Ia	231.9955	42.846861		0.0185896	0.026274	0.808231	100.692	-
9041–12702	2017dgs	II	236.38983	30.145431		0.0316281	0.0331679	0.406954	166.074	-
9043–12701	2017def	Ia	230.62042	27.707189		0.0748986	0.0407621	0.633883	164.034	+
8625–9101	2017cxz	Ib	259.83242	57.898833	PGC 140771	0.0289486	0.031763	0.414263	7.11978	-
8145–1902	2017ckx	Ia	117.04586	28.230289	UGC 04030 NED01	0.0271584	0.0341972	0.379181	81.3	-
8149–9102	2017cfq	II	120.98008	26.520167	IC 0491	0.0217485	0.0427882	0.436642	114.077	-
8547–12701	2017boa	Ia	217.63179	52.704325	SDSS J143031.19+524225.8	0.0448811	0.0114932	0.47447	164.296	+
9501–12705	2016gkm	Ib/c	130.72108	25.070919		0.0172569	0.032717	0.866949	136.132	-
9509–12703	2016acq	II	124.10248	25.993122		0.0452423	0.0354447	0.728145	127.374	+
8550–9101	2015cq	II	247.41083	40.236111	SDSS J162938.32+401407.4	0.0283296	0.00875131	0.177729	74.261	-
7960–12705	2015co	II	258.6505	30.735667	SDSS J171436.05+304400.7	0.0295939	0.0486122	0.544136	158.44	-
9027–12701	2012fj	IIP	243.93692	31.96325	NGC 6103	0.0315467	0.0229677	0.693064	74.9238	-
8453–12702	2012al	IIn	151.54837	47.294611	Anon.	0.0381068	0.0111072	0.474214	167.375	-
8588–6101	2011cc	IIn	248.456	39.263531	IC 4612	0.0317611	0.0103404	0.954619	153.413	-
7495–12702	2010ee	II	205.07496	26.353311	UGC 8652	0.0284013	0.0135025	0.189334	13.9973	-
7968–9102	2010dl	Ia	323.75404	–0.51328056	IC 1391	0.030156	0.0382006	0.750483	77.4445	+
9876–12703	2009L	Ia	194.70042	27.673781	NGC 4854	0.0279622	0.010924	0.76496	53.2682	+
8261–12705	2007sw	Ia	183.40367	46.493361	UGC 7228	0.0257328	0.0187694	0.332757	179.967	-
8080–12705	2007gl	Ib/c	47.888371	–0.74631111	Anon.	0.0282305	0.0645811	0.922932	11.7656	-
8138–12704	2007R	Ia	116.65637	44.789469	UGC 4008	0.030805	0.046767	0.625464	165.866	-
9033–12705	2007O	Ia	224.02158	45.404689	UGC 9612	0.0361875	0.0231061	0.694846	89.3529	-
9193–12704	2006np	Ia	46.6645	0.064030556	Anon.	0.107438	0.083128	0.66192	24.9588	+
7975–6104	2006iq	Ia	324.89062	10.484861	Anon.	0.0788547	0.0610815	0.87799	98.1721	-
8322–12705	2006cq	Ia	201.10458	30.956311	IC 4239	0.0485022	0.0150732	0.732988	141.256	+
9036–9102	2005bk	Ic	240.571	42.915361	MCG +07-33-27	0.0244346	0.0147117	0.950868	146.291	-
8153–12702	2004hx	II	40.3025	–0.87943889	Anon.	0.0381235	0.0338392	0.474935	71.3878	-
7990–3703	2004eb	II	262.10125	57.546031	NGC 6387	0.0285483	0.0385512	0.555031	86.9226	-
8078–12701	2004I	II	40.880129	0.30853056	NGC 1072	0.0266695	0.037467	0.381776	11.3952	+
8990–12702	2004H	Ia	173.49904	49.062919	IC 708	0.0316278	0.0195327	0.777672	168.268	+
8984–9101	2003an	Ia	201.97312	28.508111	MCG +05-32-22	0.0369943	0.0134218	0.791246	32.2228	+
8615–9102	2002ik	IIP	321.47613	0.41488889	Anon.	0.0317398	0.0545153	0.465725	82.503	-
9027–9101	2002ci	Ia	243.90812	31.3215	UGC 10301	0.0221977	0.0332517	0.247826	12.5372	-
9029–12702	2002cg	Ic	247.252	41.283439	UGC 10415	0.0318872	0.0112731	0.793745	80.5852	-
8978–6102	2002aw	Ia	249.37108	40.880639	Anon.	0.0263847	0.00693859	0.242865	79.4155	+
8323–6101	2002G	Ia	196.98025	34.085139	Anon.	0.03365	0.0126278	0.827951	60.7429	+
8604–12701	2000cs	II	245.88433	39.12475	MCG +07-34-15	0.0350385	0.0088737	0.973792	166.75	+
8588–12702	1991L	Ib/c	250.31262	39.292389	MCG +07-34-134	0.0305423	0.0144956	0.667299	79.4933	-
8250–12704	1999 gw	Unknown	138.97792	44.331944	UGC 4881	0.0397859	0.0171982	0.551148	67.5947	-
8322–3701	1996 ce	Unknown	199.06446	30.264611	Mrk785	0.0491864	0.0112192	0.803095	152.056	-
8332–1902	2005 cc	Ia pec:	209.27021	41.844944	NGC 5383	0.00814191	0.00652679	0.704969	116.136	-
8935–6104	1991 Q	Unknown	195.53163	27.648819	NGC 4926A	0.023012	0.00914655	0.490692	74.2748	-
9041–9102	2004 ct	Ia	235.94063	28.416528	M+05-37-17	0.0327509	0.0312202	0.791074	125.17	-
9044–6101	1962 B	I	230.68879	29.768944	M+05-36-25	0.0229164	0.0267391	0.759202	92.9868	-
8158-1901	ASASSN-15pn	Ia	60.85966667	–5.492027778	SDSS J040326.23-052930.6	0.0383575	0.0942628	0.489294	68.1569	-
8311–6104	Gaia15abd	Ia	205.2829583	23.283		0.0263526	0.01702	0.783214	161.689	+
8588–6102	ASASSN-15ns	Ia	250.11675	39.32021389	MRK887	0.0300793	0.013048	0.722699	17.4751	+
9043–12704	ASASSN-15mm	II	231.3479167	29.17401944	SDSS J152523.40+291018.8	0.0214421	0.0237239	0.457505	1.30472	-
9510–9101	ASASSN-15uv	Ia	126.783875	27.81159444	2MASX J08270817+2748382	0.0202794	0.0332955	0.402262	13.8534	-
7815–3702	2017frb	Ia	317.9034583	11.49724444	CGCG426-012	0.0293823	0.101375	0.853027	170.98	-
8550–12705	1975K	Unknown	249.13713	39.030139	NGC 6195	0.029986	0.0185899	0.597257	38.9863	+

same as in Zhou et al. (2019). See Zhou et al. (2019) for more details.

We estimate the dust extinction using Hα and Hβ emission line ratios (Osterbrock & Ferland 2006) and the equation $Rv = Av/E(B-V)$ (Fitzpatrick 1999). Then we do dust extinction correction for the emission line fluxes in the line of sight direction through galaxies.

According to Kennicutt (1998), we estimate the ongoing SFR from Hα luminosity. We calculate the global SFR by summing the SFR of all the single spaxels in 1.5 R_e of galaxies.

There are several methods to estimate the gas-phase oxygen abundance (Stasińska 2006; Izotov et al. 2006; Liang et al. 2006, 2007; Yin et al. 2007). Here we utilize strong line methods of O3N2 (Alloin et al. 1979; Pettini & Pagel 2004), N2O2 (Liang et al. 2006; Dopita et al. 2000, 2013; Zhang et al. 2017) and R23 (Pilyugin & Thuan 2005; Pagel et al. 1979; McGaugh 1991; Zaritsky et al. 1994; Tremonti et al. 2004; Kewley & Dopita 2002; Kobulnicky & Kewley 2004; Pilyugin 2001) to obtain the global and local gas-phase oxygen abundance of SN host galaxies.

3 RESULTS

The global properties are estimated using emission line fluxes from MaNGA DAP of all the useful spaxels in 1.5 R_e of galaxies. The central and SN location properties are estimated using emission line fluxes of the spaxels within a circular region of 2.5 arcsec radius around the galaxy centers and SN explosion positions. The global SFR and gas-phase oxygen abundance for galaxies without AGNs in the galaxy centers are estimated considering emission line fluxes of spaxels in 1.5 R_e of galaxies. While for galaxies with AGNs in the galaxy centers, the global SFR and gas-phase oxygen abundance are estimated with emission line fluxes of spaxels within 1.5 R_e after excluding spaxels in central regions. In this section, firstly we will present the locations of galaxy centers in the BPT diagnostic diagram in Figure 3 to check if there are AGN components in galaxy centers. Then we will compare the global properties of the host galaxies of SNe Ia and CCSNe and the results will be shown from Figure 4 to Figure 11. Also, we will compare the local galaxy properties at the SN explosion locations and display the results in Figure 12 and Figure 13. Table 2 provides the median and mean values of the global and local properties for the SN host galaxies in our sample.

3.1 BPT Diagnostic Diagram

To some extent, the existence of AGNs will bias the measurements. For galaxies with AGNs in the centers, the central regions should be excluded when calculating the global SFR and gas-phase oxygen abundance. Due to different excitation mechanisms, AGNs can be distinguished well from star forming galaxies by the BPT diagram, which depicts the flux ratio distribution of log([N II] λ6583/Hα) on the horizontal axis and log([O III] λ5007/Hβ) on the vertical axis (Baldwin et al. 1981).

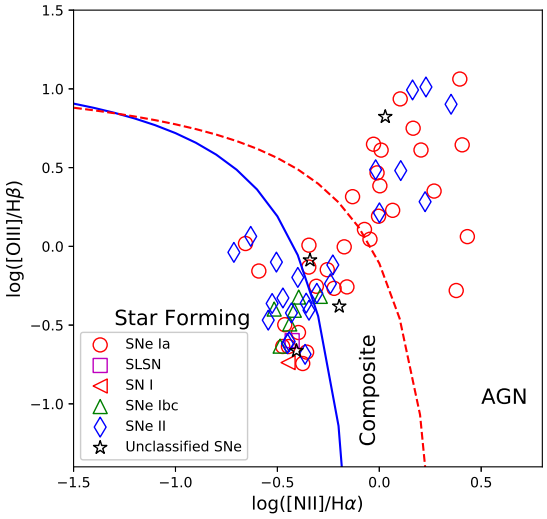

Fig. 3 The BPT diagram for our sample galaxies. We plot the emission-line flux ratio of log([O III]/Hβ) versus the ratio log([N II]/Hα) for the central regions of all the galaxies in our sample. Different symbols represent different types of SNe.

Figure 3 presents the locations of the central regions of our sample galaxies in the BPT diagram. In this figure, different symbols represent different types of SNe. According to Figure 3, there are 25 sample galaxies with AGNs in the center. In Table 1, we use '+' to signify that there are AGNs in the center of a galaxy and '-' to represent a galaxy without AGNs. See details in Table 1. The number ratios of Type Ia, CCSN and unclassified types of SN host galaxies with AGNs in the center are 0.53 (17/32), 0.24 (7/29) and 0.25 (1/4), respectively. To reduce the impact of AGNs on global properties, we exclude the central regions of these 25 sample galaxies when estimating the global SFR and gas-phase oxygen abundance.

3.2 The Difference in Global Properties between Different Types of SNe Host Galaxies

We estimate the global SFR through Hα flux by summing the SFR of each useful spaxel in SN host galaxies. Figure 4 shows the cumulative distribution of global SFR

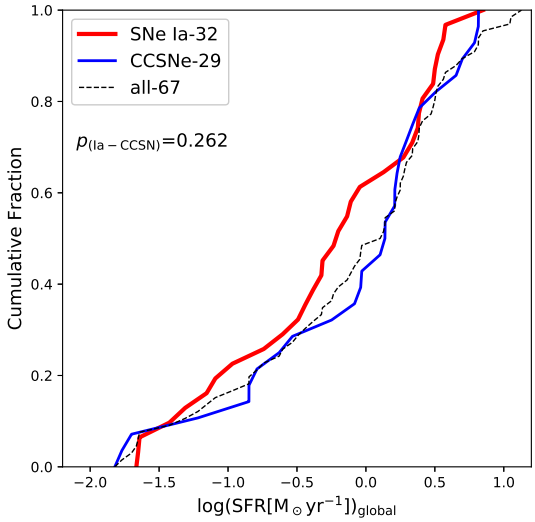

Fig. 4 The cumulative distributions of global SFR for different types of SN host galaxies.

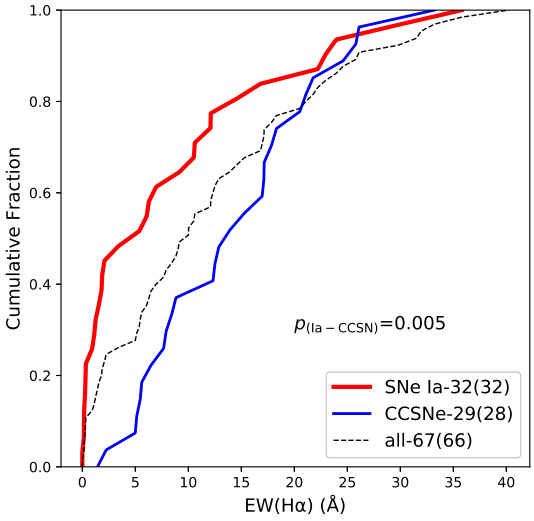

Fig. 5 The cumulative distributions of global EW(Hα) for different types of SN host galaxies.

for Type Ia SNe, CCSN and all the sample galaxies, which are marked with red thick solid lines, blue thin solid lines and black dashed lines, respectively. We apply a Kolmogorov-Smirnov (K-S) test between SNe Ia and CCSN host galaxies. According to the p-value of the K-S test, which is 0.262, we can see that there is a difference between the global SFR distribution of SNe Ia and that of CCSN host galaxies. SNe Ia can explode in both late-type star forming galaxies and early-type galaxies, but CCSNe only explode in star forming galaxies. We can see from Figure 4 and Table 2 that the average SFR of CCSN host galaxies is higher than that of SN Ia host galaxies, which means that CCSN host galaxies have stronger star forming activities.

The equivalent width of Hα (EW(Hα)) is thought to be an indicator of the strength of ongoing SFR compared with the past SFR (Sánchez et al. 2013; Galbany et al. 2014). In this work, the global EW(Hα) is estimated by calculating the median value of the spaxels in 1.5 R_e of galaxies. We present the cumulative distributions of the global EW(Hα) for SN Ia and CCSN host galaxies in Figure 5. According to the p-value of the K-S test, there is a significant difference between the global EW(Hα) of these two types of SN host galaxies. From Figure 5 and Table 2, we can see that the EW(Hα) of CCSN host galaxies is higher than that of SN Ia hosts.

The cumulative distributions of global gas-phase oxygen abundance for different types of SN hosts are presented in Figure 6. Here the gas-phase oxygen abundance is estimated using the O3N2 method. From the K-S test, we can see that there is a high probability

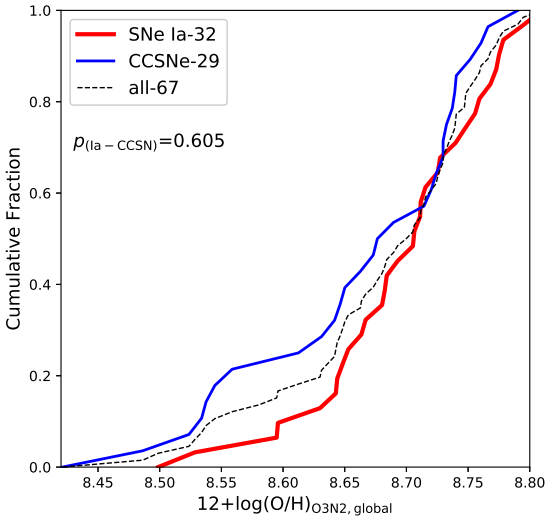

Fig. 6 The cumulative distributions of global gas-phase oxygen abundance for different types of SN host galaxies.

(p = 0.605) for SN Ia and CCSN hosts with the same distribution, which means the difference in global gas-phase oxygen abundance between SN Ia and CCSN hosts is small.

Here we adopt the stellar mass from NSA, which can provide the stellar mass of the whole galaxy. It is estimated based on the photometry image of the whole galaxy. The cumulative distributions of global stellar mass for different types of SN hosts are depicted in Figure 7. From this figure we can see that the stellar mass of our sample

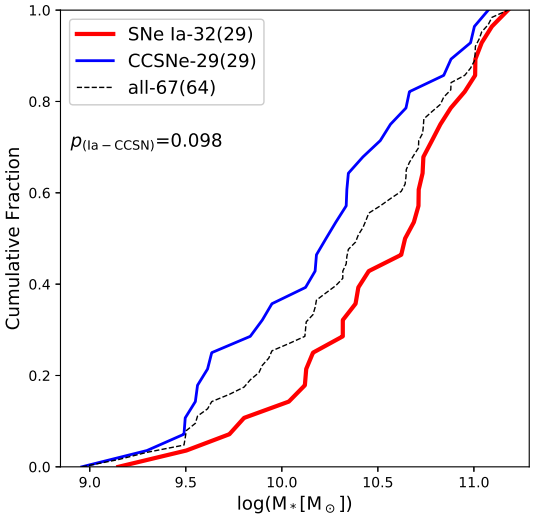

Fig. 7 The cumulative distributions of global stellar mass for different types of SN host galaxies.

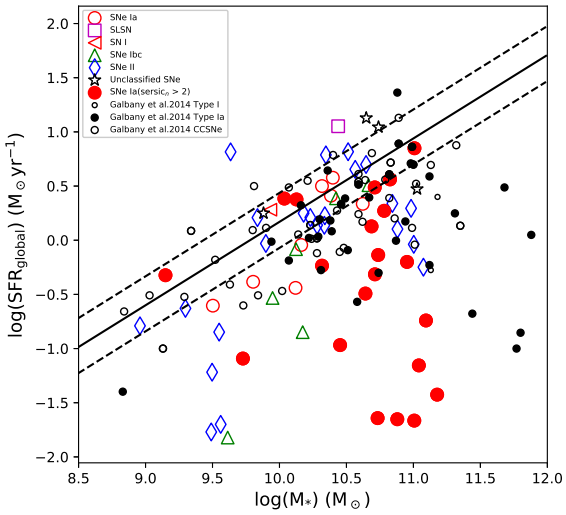

Fig. 8 The relation between global stellar mass and SFR for different types of SN host galaxies.

galaxies ranges from 10^9 to $10^{11.5}$ $M_\odot$. Only less than 20% of SNe Ia and 30% of CCSNe are found to explode in galaxies with stellar mass lower than 10^{10} $M_\odot$. This can be explained by the way of searching for nearby SNe, which are often observed by targeting bright massive galaxies. Thus, galaxies with lower stellar mass are unrepresentative for the nearby SN sample (Kelly et al. 2010; Neill et al. 2009; Arcavi et al. 2010; Galbany et al. 2014). According to the p-value of the K-S test, there is a significant difference in the stellar mass between SN Ia hosts and CCSN hosts. From this figure and Table 2, SN Ia hosts are more massive by ∼0.3 dex than CCSN hosts on average.

We present the relation between stellar mass and global SFR for our sample galaxies and that for sample galaxies from Galbany et al. (2014) in Figure 8. We should note that the stellar mass adopted for our sample galaxies is that of the whole galaxies, while the global SFR is for the part of galaxies within 1.5 R_e of galaxies. We can see that most of our sample galaxies are located close to the relation defined by Elbaz et al. (2007) and Brinchmann et al. (2004), who studied star forming galaxies with redshift ∼0 from SDSS data. There are some galaxies with higher stellar mass and lower SFR that deviate largely from the locus of Elbaz et al. (2007). Most of these galaxies are the hosts of SNe Ia. On the whole, the relation for our sample galaxies is consistent with that of some literatures (Brinchmann et al. 2004; Elbaz et al. 2007; Galbany et al. 2014; Zhou et al. 2019).

We present the distributions of stellar mass for all the galaxies and global gas-phase oxygen abundance and compare them with those of Tremonti et al. (2004) in Figure 9. Here we choose gas-phase oxygen abundance estimated with the R_{23} method because the measurements in the relation in Tremonti et al. (2004) are estimated via the R_{23} method. In this figure, the larger symbols represent galaxies with AGNs in the center. From this figure, we can see that most of our sample galaxies are located within or near the region of 95% level determined by Tremonti et al. (2004). Some massive galaxies deviate slightly from the 95% level and they have lower global gas-phase oxygen abundance. These massive galaxies mostly host SNe Ia and there are AGNs in the centers of galaxies. The relation between stellar mass and gas-phase oxygen abundance in Tremonti et al. (2004) is only for star-forming galaxies in SDSS. However, for some of our SN host galaxies, especially for some SNe Ia, their host galaxies are ellipticals. In our sample, there are AGNs in the central regions for 25 SN hosts. When estimating the gas-phase oxygen abundance, we remove out the central regions for galaxies with AGNs in the centers. Therefore, the global gas-phase oxygen will be lower and located below the lines of Tremonti et al. (2004).

Also, the deviation may be caused by the systematic difference between the procedure for stellar mass and gas-phase oxygen abundance estimation. In our work, we estimate the gas-phase oxygen abundance by calculating the median value of the spaxels with emission line fluxes in 1.5 R_e of galaxies. However, Tremonti et al. (2004) use SDSS single-fiber spectra to obtain the gas-phase oxygen abundance. Therefore, our result may be systematically lower than that in Tremonti et al. (2004). The stellar mass in our work is derived from NSA, which is based on the

Table 2 The median and mean values with standard deviations of the local and global properties for host galaxies of SNe Ia, CCSNe and all the sample galaxies.

SN Type	Global		Local	
	median	mean	median	mean
	$\log(SFR)$ $[M_\odot\ \mathrm{yr}^{-1}]$		$\log(\Sigma_{SFR})$ $[M_\odot\ \mathrm{yr}^{-1}\ \mathrm{kpc}^{-2}]$	
SNe Ia	–0.24 ± 0.73	–0.30 ± 0.73	–2.15 ± 1.34	–2.54 ± 1.34
CCSNe	0.14 ± 0.76	–0.14 ± 0.76	–2.17 ± 1.10	–2.57 ± 1.10
All	0.12± 0.77	–0.13 ± 0.77	–2.10 ± 1.19	–2.49 ± 1.19
	$\log(M_*)$ $[M_\odot]$			
SNe Ia	10.63 ± 0.49	10.47 ± 0.49	...	...
CCSNe	10.26 ± 0.56	10.18 ± 0.56	...	...
All	10.39 ± 0.54	10.34 ± 0.54	...	...
	$\mathrm{EW}_{\mathrm{H}\alpha}$ [Å]			
SNe Ia	5.78 ± 8.84	8.14 ± 8.84	4.08 ± 11.18	9.33 ± 11.18
CCSNe	14.65 ± 16.66	16.65 ± 16.66	21.23 ± 13.97	23.60 ± 13.97
All	10.20 ± 13.87	13.11 ± 13.87	12.60 ± 14.80	16.67 ± 14.80
	$\mathrm{H}\delta_\mathrm{A}$ [Å]			
SNe Ia	1.84 ± 2.28	2.15 ± 2.28	1.83 ± 2.46	2.05 ± 2.46
CCSNe	4.38 ± 1.56	4.10 ± 1.56	4.61 ± 1.33	4.53 ± 1.33
All	3.92 ± 2.18	3.32 ± 1.98	4.06 ± 2.39	3.46 ± 2.39
	Dn(4000)			
SNe Ia	1.56 ± 0.28	1.59 ± 0.28	1.50 ± 0.41	1.48 ± 0.41
CCSNe	1.32 ± 0.21	1.32 ± 0.21	1.32 ± 0.12	1.34 ± 0.12
All	1.32 ± 0.28	1.44 ± 0.28	1.37 ± 0.30	1.41 ± 0.30
	12+log(O/H) O3N2			
SNe Ia	8.71 ± 0.07	8.69 ± 0.07	8.72 ± 0.10	8.71 ± 0.10
CCSNe	8.68 ± 0.09	8.66 ± 0.09	8.74 ± 0.11	8.68 ± 0.11
All	8.70 ± 0.08	8.68 ± 0.08	8.72 ± 0.10	8.70 ± 0.10
	12+log(O/H) N2O2			
SNe Ia	8.96 ± 0.09	8.96 ± 0.09	8.97 ± 0.11	8.97 ± 0.11
CCSNe	8.91 ± 0.11	8.90 ± 0.11	8.94 ± 0.12	8.92 ± 0.12
All	8.95 ± 0.10	8.93 ± 0.10	8.96 ± 0.11	8.95 ± 0.11
	12+log(O/H) R_{23}			
SNe Ia	8.91 ± 0.07	8.91 ± 0.07	8.88 ± 0.15	8.90 ± 0.15
CCSNe	8.88 ± 0.10	8.88 ± 0.10	8.92 ± 0.13	8.91 ± 0.13
All	8.89 ± 0.10	8.89 ± 0.10	8.92 ± 0.14	8.90 ± 0.14

photometry image of the whole galaxy and can hence provide us the mass of the whole galaxy, while the mass from Tremonti et al. (2004) is based on the method in Kauffmann et al. (2003b), which is measured based on a single fiber spectrum of the nucleus and then scaled to the whole galaxy.

Dn(4000) is well known as an indicator for stellar population age (Bruzual et al. 1983; Balogh et al. 1999; Kauffmann et al. 2003a). In our work, the global Dn(4000) and $\mathrm{H}\delta_\mathrm{A}$, which will be described below, are estimated by calculating the median value of spaxels within $1.5\ R_e$ of galaxies. We present the cumulative distributions of the global Dn(4000) for different types of SN host galaxies in Figure 10. From this figure we can see that there is a significant difference in global Dn(4000) between SN Ia and CCSN hosts. On average, the Dn(4000) of SN Ia hosts is larger than that of CCSN hosts, which means that the stellar population of SN Ia hosts is older than that of CCSN hosts.

$\mathrm{H}\delta_\mathrm{A}$ can also trace the stellar population of galaxies (Worthey et al. 1997). In Figure 11, we present the relations between Dn(4000) and $\mathrm{H}\delta_\mathrm{A}$ for our sample galaxies and compare them with Kauffmann et al. (2003b), who studied pure burst star formation histories and continuous star formation histories with different metallicities. From Figure 11, we can see that the relations for our sample galaxies are quite consistent with those of Kauffmann et al. (2003b). In this relation, the global values of Dn(4000) for SN Ia host galaxies are larger than those of CCSN host galaxies and the global values of $\mathrm{H}\delta_\mathrm{A}$ for SN Ia host galaxies are lower than those for CCSN host galaxies, which means that the stellar population of CCSN host galaxies is younger than that of SN Ia hosts. This result is consistent with the cumulative distribution of Dn(4000).

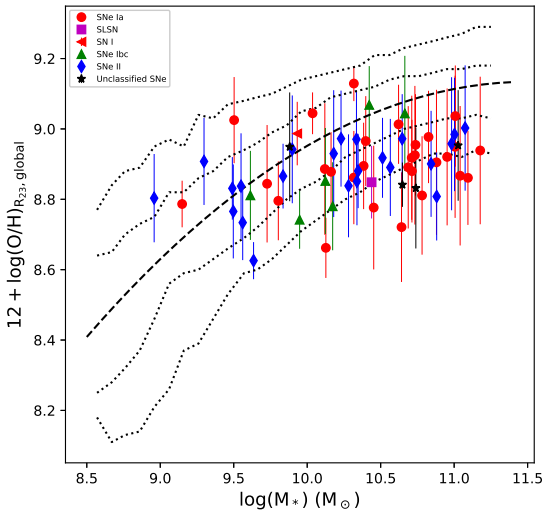

Fig. 9 The relation between global stellar mass and gas-phase oxygen abundance estimated by R_{23} for different types of SN host galaxies.

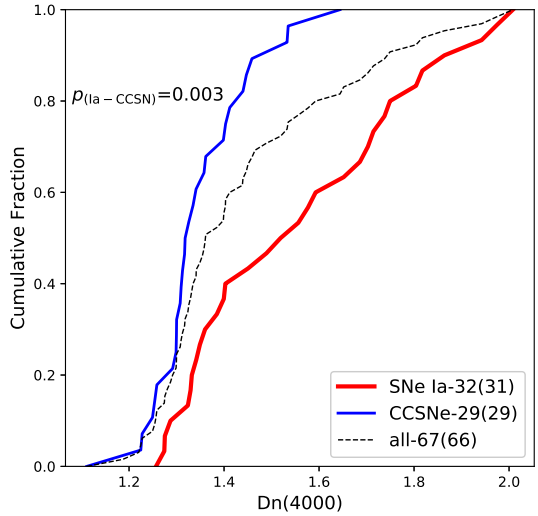

Fig. 10 The cumulative distributions of global Dn(4000) for different types of SN host galaxies.

3.3 The Difference in Local Properties between Different Types of SN Host Galaxies

We estimate the local properties of SN explosion sites considering emission line fluxes of useful spaxels in a circular region with a radius of 2.5 arcsec. Figure 12 shows the cumulative distributions of local star formation density (ΣSFR) at the SN explosion sites. We obtain a high p-value for the K-S test (p = 0.70), which means that there is

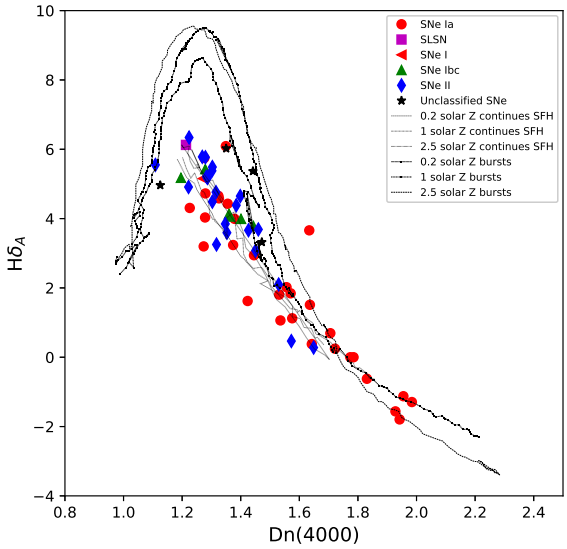

Fig. 11 The distribution of the global Dn(4000) and H$\delta_{\rm A}$ for our SN galaxies. The dashed and chain lines are the relations between Dn(4000) and H$\delta_{\rm A}$ for 20% solar, solar and 2.5 times solar metallicity bursts, respectively. The dotted lines are the relations between Dn(4000) and H$\delta_{\rm A}$ for 20% solar, solar and 2.5 solar metallicity continuous star formation histories. These lines are taken from Kauffmann et al. (2003b).

no significant difference between the local ΣSFR of SN Ia explosion sites and that of CCSN.

In Figure 13, the cumulative distributions of local gas-phase oxygen abundance for different types of SN

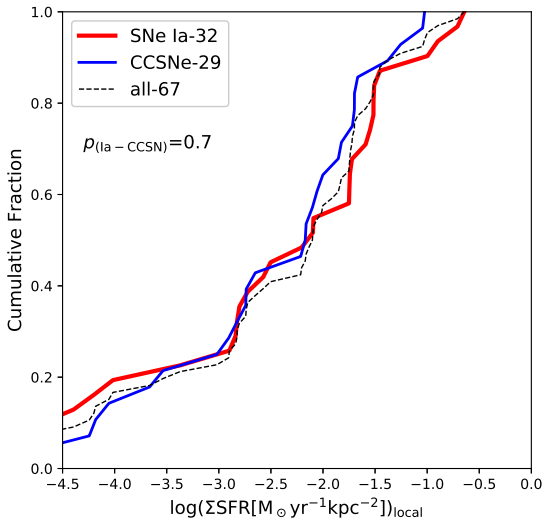

Fig. 12 The cumulative distributions of local ΣSFR for different types of SN host galaxies at SN explosion sites.

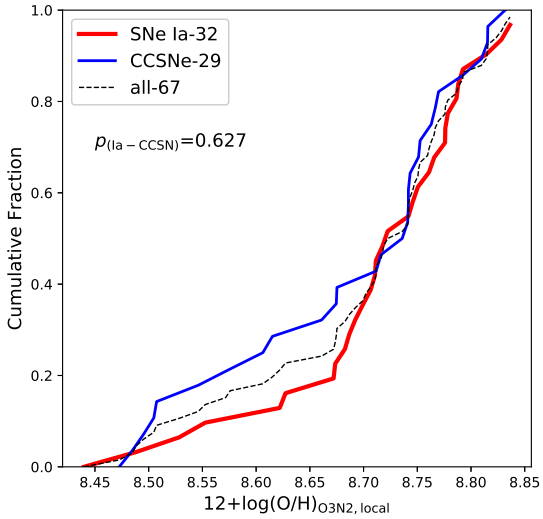

Fig. 13 The cumulative distributions of local gas-phase oxygen abundance for different types of SN host galaxies at SN explosion sites.

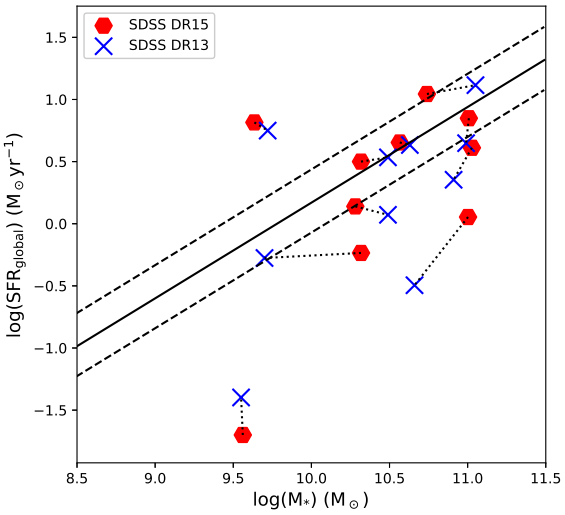

Fig. 14 The relations of global SFR and stellar mass for the same sample galaxies for DR13 in Zhou et al. (2019) and DR15 data in this paper.

explosion sites are presented. From this figure, we can see that the local gas-phase oxygen abundance of SN Ia explosion sites is slightly higher than that of CCSNe on average. In general, there is no significant difference between the local gas-phase oxygen abundance at the explosion sites for different types of SNe.

4 DISCUSSION

4.1 Comparisons with the Measurements in DR13

We compare the distributions of stellar mass and SFR of galaxies in DR15 in this work with those in DR13 studied by Zhou et al. (2019) in Figure 14 for the same sample objects. The red hexagons and blue pluses represent measurements in DR15 and DR13, respectively. The stellar masses in DR15 are derived from NSA and those in DR13 are estimated using `STARLIGHT` code. From this figure, we can see that the relations between stellar mass and SFR for DR15 data are very consistent with those for DR13 data in Zhou et al. (2019).

In Figure 15, the relations between stellar mass and global gas-phase oxygen abundance estimated by the R_{23} method for the same sample galaxies in both Zhou et al. (2019) and this work are presented. We can see that the difference between the present measurements in DR15 and those in DR13 is small. All of the same sample galaxies are located within or nearby the lines that enclose 95% of the data from Tremonti et al. (2004).

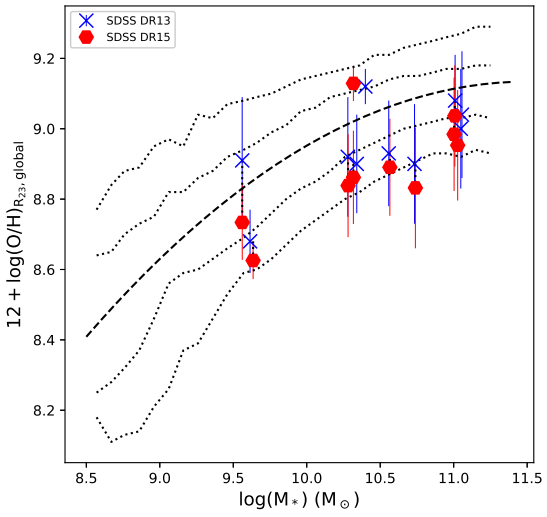

Fig. 15 The relations of global gas-phase oxygen abundance and stellar mass for the same sample galaxies for DR13 in Zhou et al. (2019) and DR15 data in this paper.

4.2 The Difference between Local and Global Gas-phase Oxygen Abundance for Our Sample Galaxies

The specific local properties of SN explosion sites are important to derive the properties of progenitors. However, for some SNe exploding in distant galaxies, whose spectra can often be obtained with long-slit or fixed aperture

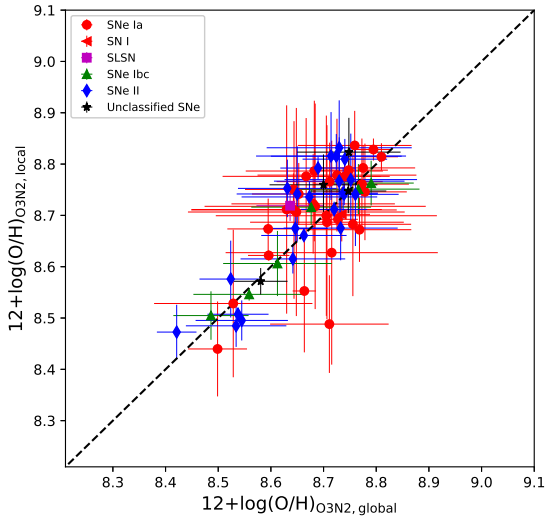

Fig. 16 The difference between local and global gas-phase oxygen abundance for different types of SN host galaxies.

fibers, only global properties of galaxies can be measured. Therefore, we try to study the correlation between local and global properties. According to the correlation, we can estimate the local properties of SN explosion sites through the global properties. Due to our sample limitation that there is a lack of low mass host galaxies, we can employ IFU data to investigate the difference between local and global properties for now.

Here we should note that the progenitors of SNe Ia may be very old stars (Maoz et al. 2011) and the local properties at their recent locations may be different from those of the regions where they originally formed, which is because they may have migrated from their birth place.

The difference between local and global gas-phase oxygen abundance is shown in Figure 16. From this figure we can see that most of our sample galaxies are located close to the dashed line, which represents the ratio of local and global gas-phase oxygen abundance being 1:1. This is consistent with Galbany et al. (2016b) and Zhou et al. (2019). There are some galaxies that deviate slightly from the dashed line and most of these galaxies host SNe Ia.

4.3 The Differences of Measurements between Different Types of SN Host Galaxies

Through the cumulative distributions of global SFR, we can see that for our sample galaxies, CCSNe tend to explode in hosts with higher SFR than SNe Ia. As Kennicutt (1998) and Gogarten et al. (2009) pointed out, massive stars, which are thought to be the progenitors of CCSNe, explode near the sites where they are born and their lifetimes are shorter than less massive stars. The explosion of massive stars could cause the decrease of Hα emission intensity and peculiar motions of less massive stars around them (Eldridge et al. 2011). Then the less massive stars would explode to SNe Ia in lower Hα emission environments that are further away from the centers of star formation regions. SNe Ia can be observed both in ellipticals and in spiral galaxies, which contain old and young stellar populations (Kehrig et al. 2012). Therefore, the SFR of SN Ia hosts is lower than that of CCSN hosts on average.

In our sample, SN Ia hosts are more massive than CCSN hosts on average. The mean logarithmic stellar mass for SN Ia host galaxies is 10.47$\pm$0.49 and 10.18$\pm$0.56 for CCSN hosts. The difference in stellar mass between SN Ia and CCSN hosts is $\sim$0.3 dex on average. This indicates that the ratio of CCSNe to SNe Ia will decrease with increasing stellar mass of galaxies, which is consistent with Galbany et al. (2014). As Galbany et al. (2014) pointed out, this can be explained by the different delay-time distribution (DTD) for SNe Ia and CCSNe. About half of the progenitors of SNe Ia are older than 1 Gyr (Maoz et al. 2010, 2011), while CCSNe explode within about 40 Myr after star formation. There is a positive relation between SFR and stellar mass within 10^{11} $M_{\odot}$ (Elbaz et al. 2007). Compared with less massive galaxies, there is a larger fraction of old stellar populations in more massive galaxies. Therefore, the ratio of CCSNe to SNe Ia will decrease with the stellar mass of galaxies increasing.

The difference of both global and local gas-phase oxygen abundance between SN Ia and CCSN hosts is small for our sample. The average global gas-phase oxygen abundance estimated by the O3N2 method for SN Ia and CCSN hosts is 8.69 and 8.66, respectively. The mean local gas-phase oxygen abundance for both types is 8.71 and 8.68, respectively. The differences both for global and local are significantly smaller than 1σ.

5 CONCLUSIONS

In this work, we present the local and global properties, including SFR, gas-phase oxygen abundance, galaxy mass, Dn(4000), etc., for 67 different types of SN host galaxies selected from SDSS DR15 within the FoV of MaNGA. There are 32 Type Ia, 29 CCSNe, 1 SLSN, 1 Type I and 4 unclassified type of SNe in our sample. Using spatially resolved IFS of MaNGA, we could derive the cumulative distribution of the local environment of SN explosion sites and the global properties of different types of SN hosts. Also, we compare the local with global gas-phase oxygen abundance to derive the differences between them. Like our first paper of a series, Zhou et al. (2019), our sample from MaNGA has higher redshifts with a median of $\sim$0.03, which can be utilized to analyze more distant SN host

galaxies. We would like to point out that in our work, due to the limited sample size, we could not remove the mass dependence for different types of SN host galaxies, which is likely the true driver of the trends for the properties presented in this work. Our results are summarized as follows.

On average, the fact that global SFR of SN Ia host galaxies is lower than that of CCSN hosts is consistent with the results of EW(Hα), which affirms that the star formation activity for CCSN hosts is stronger than for SN Ia hosts. The mean global stellar mass of SN Ia host galaxies is $\sim$0.3 dex higher than that of CCSN hosts, which indicates that with the increasing stellar mass of galaxies, the number ratio of SNe Ia to CCSNe will increase. The global gas-phase oxygen abundance between different types of SN host galaxies is almost similar. According to the Dn(4000) distribution of different types of SN hosts, the stellar population age for SN Ia host galaxies is older than that of CCSN hosts on average.

There is no significant difference in local gas-phase oxygen abundance and local SFR density for SN Ia and CCSN explosion sites in their host galaxies. For most of our sample galaxies, the difference between global and local gas-phase oxygen abundance is small. While for some SN Ia host galaxies, the difference is larger.

There will be a larger sample of SN host galaxies in the MaNGA survey, which has observed $\sim$4600 galaxies till now, and there will be 10 000 galaxies at the end of this survey. At that time, we could obtain more and more SN hosts and make a more detailed and fair comparison between the explosion environments and progenitors of different types of SNe after removing mass dependence.

Acknowledgements We appreciate the referee who provided very constructive and helpful comments and suggestions, which helped to improve our work very much. We thank Yanbin Yang, Francois Hammer and Michel Dennefeld for helpful discussions. This work was supported by the National Science Foundation of China (Grant No.11733006 to HW, 11903046 to JG and U1631105 to WB), and by the Beijing Municipal Natural Science Foundation (No. 1204038 to JG).

Funding for the Sloan Digital Sky Survey IV has been provided by the Alfred P. Sloan Foundation, the U.S. Department of Energy Office of Science, and the Participating Institutions. SDSS acknowledges support and resources from the Center for High-Performance Computing at the University of Utah. The SDSS web site is www.sdss.org.

SDSS is managed by the Astrophysical Research Consortium for the Participating Institutions of the SDSS Collaboration including the Brazilian Participation Group, the Carnegie Institution for Science, Carnegie Mellon University, the Chilean Participation Group, the French Participation Group, Harvard-Smithsonian Center for Astrophysics, Instituto de Astrofísica de Canarias, The Johns Hopkins University, Kavli Institute for the Physics and Mathematics of the Universe (IPMU) / University of Tokyo, the Korean Participation Group, Lawrence Berkeley National Laboratory, Leibniz Institut für Astrophysik Potsdam (AIP), Max-Planck-Institut für Astronomie (MPIA Heidelberg), Max-Planck-Institut für Astrophysik (MPA Garching), Max-Planck-Institut für Extraterrestrische Physik (MPE), National Astronomical Observatories of China, New Mexico State University, New York University, University of Notre Dame, Observatório Nacional / MCTI, The Ohio State University, Pennsylvania State University, Shanghai Astronomical Observatory, United Kingdom Participation Group, Universidad Nacional Autónoma de México, University of Arizona, University of Colorado Boulder, University of Oxford, University of Portsmouth, University of Utah, University of Virginia, University of Washington, University of Wisconsin, Vanderbilt University, and Yale University.

References

Aguado, D. S., Ahumada, R., Almeida, A., et al. 2019, ApJS, 240, 23

Alloin, D., Collin-Souffrin, S., Joly, M., & Vigroux, L. 1979, A&A, 78, 200

Arcavi, I., Gal-Yam, A., Kasliwal, M. M., et al. 2010, ApJ, 721, 777

Arnett, W. D., Bahcall, J. N., Kirshner, R. P., & Woosley, S. E. 1989, ARA&A, 27, 629

Baldwin, J., Phillips, M. M., & Terlevich, R. J. 1981, PASP, 93, 5

Balogh, M. L., Morris, S. L., Yee, H. K. C., et al. 1999, ApJ, 527, 54

Barbon, R., Ciatti, F., & Rosino, L. 1979, A&A, 72, 287

Barbon, R., Buond, V., Cappellaro, E., & Turatto, M. 1999, A&AS, 139, 531

Barbon, R., Cappellaro, E., Ciatti, F., et al. 1984, A&AS, 58, 735

Barbon, R., Cappellaro, E., & Turatto, M. 1989, A&AS, 81, 421

Becker, S. A., & Iben, Jr. I. 1980, ApJ, 237, 111

Belfiore, F., Maiolino, R., Maraston, C., et al. 2016, MNRAS, 461, 3111

Bethe, H. A., Brown, G. E., Applegate, J., & Lattimer, J. M. 1979, Nucl. Phys. A, 324, 487

Blanton, M. R., Bershady, M. A., Abolfathi, B., et al. 2017, AJ, 154, 28

Brinchmann, J., Charlot, S., White, S. D. M., et al. 2004, MNRAS, 351, 1151B

Bruzual, A. G. 1983, ApJ, 273, 105

Bruzual, G., & Charlot, S. 2003, MNRAS, 344, 1000
Bundy, K., Bershady, M. A., Law, D. R., et al. 2015, ApJ, 798, 7B
Chen, T.-W., Schady, P., Xiao, L., et al. 2017, ApJL, 849, L4
Dopita, M. A., Kewley, L. J., Heisler, C. A., & Sutherland, R. S. 2000, ApJ, 542, 224
Dopita, M. A., Sutherland, R. S., Nicholls, D. C., et al. 2013, ApJS, 208, 10
Drory, N., MacDonald, N., Bershady, M. A., et al. 2015, AJ, 149, 77D
Elbaz, D., Daddi, E., Le Borgne, D., et al. 2007, A&A, 468, 33
Eldridge, J. J., Langer, N., & Tout, C. A. 2011, MNRAS, 414, 3501
Filippenko, A. V. 1997, ARA&A, 35, 309
Fitzpatrick, E. L. 1999, PASP, 111, 63
Galbany, L., Stanishev, V., Mourão, A. M., et al. 2014, A&A, 572, A38
Galbany, L., Anderson, J. P., Rosales-Ortega, F. F., et al. 2016a, MNRAS, 455, 4087
Galbany, L., Stanishev, V., Mourão, A. M., et al. 2016b, A&A, 591, A48
Galbany, L., Anderson, J. P., Sánchez, S. F., et al. 2018, ApJ, 855, 107
Gogarten, S. M., Dalcanton, J. J., Williams, B. F., et al. 2009, ApJ, 691, 115
Hamuy, M., Maza, J., Pinto, P. A., et al. 2002, AJ, 124, 417
Han, D. H., Park, C., Choi, Y. Y., & Park, M. G. 2010, ApJ, 724, 502
Hoyle, F., & Fowler, W. A. 1960, ApJ, 132, 565
Izotov, Y. I., Stasinska, G., Meynet, G., et al. 2006, A&A, 448, 955
Izzo, L., Thöne, C. C., García-Benito, R., et al. 2018, A&A, 610, A11
Kauffmann, G., Heckman, T. M., White, S. D. M., et al. 2003, MNRAS, 341, 33
Kauffmann, G., Heckman, T. M., Tremonti, C. A., et al. 2003, MNRAS, 346, 1055
Kehrig, C., Monreal-Ibero, A., Papaderos, P., et al. 2012, A&A, 540, A11
Kelly, P. L., Hicken, M., Burke, D. L., et al. 2010, ApJ, 715, 743
Kelly, P. L., & Kirshner, R. P. 2012, ApJ, 759, 107
Kewley, L. J., & Dopita, M. A. 2002, ApJS, 142, 35
Kennicutt, Jr., R. C. 1998, ARA&A, 36, 189
Kobulnicky, H. A., & Kewley, L. J. 2004, ApJ, 617, 240
Kuncarayakti, H., Doi, M., Aldering, G., et al. 2013, AJ, 146, 31
Kuncarayakti, H., Doi, M., Aldering, G., et al. 2013, AJ, 146, 30
Kuncarayakti, H., Anderson, J. P., Galbany, L., et al. 2018, A&A, 613, A35
Law, D. R., Yan, R .B., Bershady, M. A., et al. 2015, AJ, 150, 19L
Liang, Y. C., Yin, S. Y., Hammer, F., et al. 2006, ApJ, 652, 257
Liang, Y. C., Hammer, F., Yin, S. Y., et al. 2007, A&A, 473, 411
Lyman, J. D., Taddia, F., Stritzinger, M. D., et al. 2018, MNRAS, 473, 1359
Maoz, D., Sharon, K., & Gal-Yam, A. 2010, ApJ, 722, 1879
Maoz, D., Mannucci, F., Li, W., et al. 2011, MNRAS, 412, 1508
McGaugh, S. S. 1991, ApJ, 380, 140
Neill, J. D., Sullivan, M., Howell, D. A., et al. 2009, ApJ, 707, 1449
Osterbrock, D. E., & Ferland, G. J. 2006, Astrophysics of Gaseous Nebulae and Active Galactic Nuclei (Sausalito, CA: University Science Books)
Pagel, B. E. J., Edmunds, M. G., Blackwell, D. E., et al. 1979, MNRAS, 189, 95
Perlmutter, S., Aldering, G., Goldhaber, G., et al. 1999, ApJ, 517, 565
Pettini, M., & Pagel, B. E. J. 2004, MNRAS, 348, L59
Pilyugin, L. S. 2001, A&A, 374, 412
Pilyugin, L. S., & Thuan, T. X. 2005, ApJ, 631, 231
Prieto, Josẽ L., Stanek. K. Z., & Beacom. J. F. 2008, ApJ, 673, 999
Riess, A. G., Filippenko, A. V., Challis, P., et al. 1998, AJ, 116, 1009
Rubin, A., Gal-Yam, A., De Cia, A., et al. 2016, ApJ, 820, 33
Sánchez, S. F., Rosales-Ortega, F. F., Jungwiert, B., et al. 2013, A&A, 554, A58
Schlegel, E. M. 1990, MNRAS, 244, 269
Shao, X., Liang, Y. C., Dennefeld, M., et al. 2014, ApJ, 791, 57S
Stanishev, V., Rodrigues, M., Mourão, A., & Flores, H. 2012, A&A, 545, A58
Stasińska, G. 2006, A&A, 454, L127
Tremonti, C. A., Heckman, T. M., Kauffmann, G., et al. 2004, ApJ, 613, 898
Turatto, M. 2003, in Supernovae and Gamma Ray Bursters, ed. K. Weiler 598, 21, (New York: Springer)
Wake, D. 2015, in American Astronomical Society Meeting Abstracts, 225, 143.28
Wake, D. A., Bundy, K., Diamond-Stanic, A. M., et al. 2017, AJ, 154, 86
Weijmans, A.-M., & MaNGA Team 2016, Multi-Object Spectroscopy in the Next Decade: Big Questions, Large Surveys, and Wide Fields, 507, 257
Westfall, K. B., Cappellari, M., Bershady, M. A., et al. 2019, AJ, 158, 231
Worthey, G., & Ottaviani D. L., 1997, ApJS, 111, 377
Yan, R., Bundy, K., Law, D. R., et al. 2016, AJ, 152, 197
Yin, S. Y., Liang, Y. C., Hammer, F., et al. 2007, A&A, 473, 411
Zaritsky, D., Kennicutt, Jr., R. C., & Huchra, J. P. 1994, ApJ, 420, 87
Zhang, K., Yan, R., Bundy, K., et al. 2017, MNRAS, 466, 3217
Zhou, L., Liang, Y.-C., Ge, J.-Q., et al. 2019, RAA (Research in Astronomy and Astrophysics), 19, 121